Natural organic matter and ionic strength ($CaCl_2$) affect transport, retention and remobilization of silica encapsulated DNA colloids (DNAcol) in saturated sand columns

Kianfar, Bahareh; Hassanizadeh, S. Majid; Abdelrady, Ahmed; Bogaard, Thom; Foppen, Jan Willem

DOI
10.1016/j.colsurfa.2023.132476

Publication date
2023

Document Version
Final published version

Published in
Colloids and Surfaces A: Physicochemical and Engineering Aspects

Citation (APA)
Kianfar, B., Hassanizadeh, S. M., Abdelrady, A., Bogaard, T., & Foppen, J. W. (2023). Natural organic matter and ionic strength ($CaCl_2$) affect transport, retention and remobilization of silica encapsulated DNA colloids (DNAcol) in saturated sand columns. *Colloids and Surfaces A: Physicochemical and Engineering Aspects*, *678*, Article 132476. https://doi.org/10.1016/j.colsurfa.2023.132476

Colloids and Surfaces A: Physicochemical and Engineering Aspects 678 (2023) 132476

Contents lists available at ScienceDirect

Colloids and Surfaces A: Physicochemical and Engineering Aspects

journal homepage: www.elsevier.com/locate/colsurfa

Natural organic matter and ionic strength ($CaCl_2$) affect transport, retention and remobilization of silica encapsulated DNA colloids (DNAcol) in saturated sand columns

Bahareh Kianfar [a,*], S. Majid Hassanizadeh [b,c], Ahmed Abdelrady [a,1], Thom Bogaard [a], Jan Willem Foppen [a]

[a] Department of Water Management, Faculty of Civil Engineering and Geosciences, Delft University of Technology, 2628CN Delft, the Netherlands
[b] Stuttgart Center for Simulation Science (SIMTECH), Integrated Research Training Group SFB1313, Stuttgart University, Germany
[c] Department of Earth Sciences, Utrecht University, 3584CB Utrecht, the Netherlands

HIGHLIGHTS

- The retention of DNAcol was regulated by the $[Ca^{2+}]$/DOC ratio.
- There was a range of $[Ca^{2+}]$/DOC ratios with minimal DNAcol-sand interactions.
- Under transient porewater chemistry conditions, the ionic strength was a critical factor.

GRAPHICAL ABSTRACT

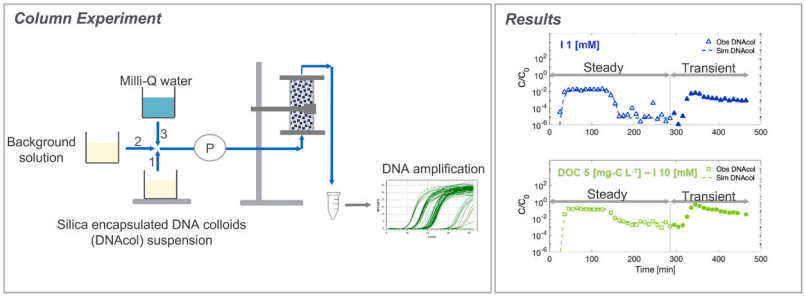

ARTICLE INFO

Keywords:
Silica-encapsulated-DNA colloid (DNAcol)
Natural organic matter (NOM)
Ionic strength ($CaCl_2$)
Remobilization
Colloidal tracer
Colloid transport

ABSTRACT

In the terrestrial environment, interactions between natural organic matter (NOM) and colloids can lead to the formation of an environmental corona around colloids, influencing their transport behaviour and, ultimately, their ecotoxicity. We used a synthetically designed colloid tagged with DNA (DNAcol) as a surrogate for natural colloids and investigated its transport in saturated sand columns. We varied the concentrations of NOM and ionic strength ($CaCl_2$), to better understand the transport and release of DNAcol in porous media under both steady and transient porewater chemistry conditions. In addition, we aimed to understand the main factors that control deposition and release of DNAcol under tested conditions. To induce transient chemistry, we replaced the injection solution containing NOM and/or $CaCl_2$ with Milli-Q water. The results showed that the deposition rate of DNAcol was inversely proportional to the concentration of NOM. The deposition rate increased significantly even under low ionic strength ($CaCl_2$) conditions of tested conditions. Notably, the influence of NOM on the transport of DNAcol was most pronounced at the lowest range of $[Ca^{2+}]$/DOC ratios, and the attachment of DNAcol to the sand grains was negligible. Moreover, the results showed while the DLVO theory captured the general trend of experimental results, it significantly underestimated the deposition of DNAcol in the presence of $CaCl_2$. Under transient porewater chemistry conditions, colloid remobilization was observed upon flushing the column with

* Corresponding author.
E-mail address: b.kianfar@tudelft.nl (B. Kianfar).
[1] Wetsus, European Center of Excellence for Sustainable Water Technology, Oostergoweg 9, 8911 MA, Leeuwarden, the Netherlands

https://doi.org/10.1016/j.colsurfa.2023.132476
Received 28 June 2023; Received in revised form 6 September 2023; Accepted 27 September 2023
Available online 29 September 2023

Milli-Q water, leading to a secondary peak in the breakthrough curves. We observed that under transient porewater chemistry conditions, when the ionic strength of the solution was 10 mM, the magnitude of the remobilization peak was more significant compared to conditions with 1 mM ionic strength. Our work emphasized the complex interplay between water quality on the one hand and deposition and release of colloidal matter in saturated porous media on the other hand.

1. Introduction

Predicting the fate and transport of engineered and biological colloidal matter in the environment has been proven to be essential in a variety of applications, including human health, and ecological risk management [1–3]. However, predicting the fate and transport of nanoparticles remains challenging, in particular in the natural environment [4].

The understanding of the transport and fate of colloidal matter in heterogeneous subsurface environments faces a primary challenge because the transport of colloidal matter is highly sensitive to chemical conditions of the subsurface environment. These conditions encompass factors such as pH [5], ionic strength [6–9] ion composition [10–12], and the presence of natural organic matter (NOM; e.g.,[13–16]). Such chemical factors can impact deposition, as well as hetero- and homo-aggregation of colloidal matter, which is potentially leading to uncertainties in risk management.

NOM such as humic and fulvic substance, proteins, and extracellular polymeric substances can adsorb onto the surface of colloids, acting as surfactant- or polymer-coating material, and forming a soft-corona or environmental corona [15,17–20]. Adsorption of those macromolecules onto the surface of colloids can impact their stability [16,21–23], transport [6,13,15,16,21,22,24–32], and, ultimately, their eco-toxicity [31,33]. Several studies have mentioned that the effect of NOM on the transport of the colloids is sensitive to various environmental factors, such as pH [13,15,27,34,35], ionic strength [13,36], and ion composition [27]. Furthermore, atomic force microscopy showed that the thickness and mass of the adsorbed layer on the surface of particle (silver) and collector (mica) was dependent on ionic strength (as presence of Ca^{2+}) of the system, and the effects were different for particle and collector [19].

Another critical environmental implication of colloidal matter is related to its remobilization as a consequence of alterations in porewater chemistry or subsurface flow conditions. Previous research in this field has indicated that colloid release can occur due to variations in ionic strength and flow conditions [9,13,37–48]. In addition, the primary mechanisms and factors governing the deposition and transport of colloidal matter under steady and transient conditions may differ [47].

Specifically, changes in the ionic strength of porewater can impact the surface charge of both colloids and collectors, subsequently affecting the magnitude of the electrical double-layer energy and, consequently, the adhesive force. Furthermore, changes in ionic strength can influence the “zone of colloid-collector interaction”, a fraction of surface area where repulsive forces can be reduced or eliminated [49–51]. This suggests that under unfavourable conditions in the presence of a strong repulsive energy barrier, predicted by mean-field DLVO theory, the interaction can become locally favourable, depending on the extent of the heterodomain area occupying the zone of colloid-collector interaction [51,52].

While a significant number of studies have focused on understanding the specific effects of physico-chemical environmental factors on the transport behaviour of colloidal matter under steady conditions, there has been less emphasis on systematically examining the mechanisms responsible for the release of colloidal particles under transient porewater chemistry conditions.

In this study, we used DNAcol, which consisted of silica-encapsulated-DNA particles [53], as a surrogate for colloidal particles. The primary advantage of DNAcol lies in its ability to extend the lower detection limit to the ppb level, due to the embedded DNA molecules on it [54]. Consequently, it might allow us to use it as a substitute for colloidal particles, addressing the challenge associated with colloidal detecting limits. Recently, more research focused on the applications of silica encapsulated-DNA in the subsurface [55–59].

In this study, we used DNAcol with the primary objective of enhancing our understanding of the individual and combined impacts of NOM and ionic strength ($CaCl_2$) on the transport, retention/attachment, and release of DNAcol under both steady and transient porewater chemistry conditions. This involved determining the attachment rate of DNAcol and evaluating its sticking efficiency. Additionally, our goal was to gain deeper insights into the impact of two tested factors, NOM and ionic strength ($CaCl_2$), on attachment/retention and release of DNAcol for steady and transient porewater chemistry conditions.

2. Materials and methods

2.1. DNAcol

DNAcol was composed of a silica core, a layer of double-stranded DNA molecules, and a silica shell that protected DNA. DNAcol was fabricated and provided by the Functional Materials Laboratory at ETH Zurich. Details of DNAcol fabrication and quantification were described in [53]. In brief, DNAcol had a SiO_2 core and SiO_2 shell. The silica core was dispersed in isopropanol *N*-trimethoxysilylpropyl-*N,N,N*-trimethylammonium chloride (TMAPS) to alter its surface charge to a positive state [53]. Subsequently, a negatively charged double-stranded DNA (dsDNA) was added to adsorb DNA onto the functionalized silica surface [53]. Then, TMAPS was applied, and, to complete the process, a silica layer was added onto the dsDNAs-silica particle using tetraethoxysilane (TEOS) [53]. After the fabrication process, using ball milling, the agglomerated particles were broken down into individual particles. The mass density and refractive index of DNAcol were assigned to be 2.2 g cm^{-3} and 1.458, respectively [60]. Prior to using DNAcol, in order to ensure that there was no free DNA, the suspension was washed by adding 0.1 μl bleach to 1 mL of stock particle suspension. Then, the suspension was centrifuged at 60,000 g for 6 min, the supernatant was removed, and the particle pellet was washed and re-suspended in Milli-Q water three times.

2.2. Stock solution and organic matter characterization

NOM used in this study was provided by Vitens, a Dutch drinking water company, and was extracted from groundwater [61]. The NOM molecular weight distribution (M_w) of the stock was similar to Caltran, et al. [61]. The NOM concentration of the prepared stock solution was determined using the combusting technique with a Total Organic Carbon Analyzer (TOC, VCPN, Shimadzu, Japan), and the concentration of organic matter we finally reported as dissolved non-purgeable organic carbon in mg DOC L^{-1} (mg-C L^{-1}). DNAcol was suspended in nine different solutions. The electrolyte stock solutions were prepared from Milli-Q water (resistivity 18 MΩ.cm, TOC $<$ 3 ppb, Millipore, Switzerland), $CaCl_2.2\ H_2O$ was added to reach average ionic strengths *(I)* of 0 (no addition), 1 mM and 10 mM. The concentration of NOM was adjusted to achieve a DOC concentration of 0 (no addition), 5 and 20 mg-C L^{-1} (Table 1). All solutions were stored at 4 °C.

About 30 min before each column experiment DNAcol suspensions were prepared by spiking DNAcol into a 70 mL aliquot of stock solution,

Table 1
The average ζ-potential, and d_h with the corresponding polydispersity index (PDI) of DNAcol in various background solutions.

(I)	*(DOC)*	Abbreviation	*ζ-Potential*	*d_h*	*PDI*
[mM]	[mg-C L^{-1}]		[mV]	[nm]	[-]
Milli-Q water	-	Milli-Q water	-33.6 ± 6.1	311 ± 8.5	0.24
Milli-Q water	-	Milli-Q water	-34.4 ± 5.3		
1	-	I1	-17.1 ± 5.7	303 ± 14	0.26
1	-	I1	-20.9 ± 6.0		
10	-	I10	-16.8 ± 8.4	302 ± 4	0.26
10	-	I10	-19.7 ± 7.6		
Milli-Q water	5	DOC5	-47.0 ± 11.1		
Milli-Q water	5	DOC5	-40.5 ± 7.6		
1	5	DOC5-I1	-22.7 ± 4.6		
1	5	DOC5-I1	-23.3 ± 5.2		
10	5	DOC5-I10	-21.9 ± 7.8		
10	5	DOC5-I10	-20.1 ± 8.6		
Milli-Q water	20	DOC20	-49.7 ± 13.4	302 ± 9	0.24
Milli-Q water	20	DOC20	-50.8 ± 7.4		
1	20	DOC20-I1	-25.0 ± 6.1	297 ± 6	0.24
1	20	DOC20-I1	-26.2 ± 6.3		
10	20	DOC20-I10	-22.3 ± 8.0	301 ± 9	0.25
10	20	DOC20-I10	-21.3 ± 8.4		

and then vortexed (3 × 10 s). Final concentration was ~1 mg L^{-1}.

2.3. Characterization of DNAcol

The effect of solution chemistry on the stability of DNAcol was assessed with zeta potential (ζ-potential) and hydrodynamic diameter (d_h), using a ZetaSizer nano (Nano Series, Malvern Instrument Ltd., Worcestershire, UK) for freshly prepared DNAcol concentrations of 10 mg L^{-1}.

2.3.1. Hydrodynamic diameter (d_h)

Hydrodynamic diameter of DNAcol was measured using a Zetasizer (Zetasizer Nano S, Malvern Instr., UK) by dynamic light scattering at a backscatter light angle of 173°, a laser beam with wavelength of 633 nm, and temperature of 25 °C, using a square polystyrene cuvette (DTS0012). The d_h of DNAcol in every suspension was measured periodically 5 times over a 120 min approximate time frame. All measurements were carried out in a triplicate sequential auto-run for a duration of 60 s. The d_h was reported as a Z-average (Z-Ave) diameter with a corresponding polydispersity index (PDI), determined from the intensity autocorrelation function available in the Zetasizer software.

2.3.2. Zeta-potential (ζ-potential)

The zeta potential (ζ-potential) of DNAcol was determined with the same Zetasizer indirectly from electrophoretic mobility measurements at 25 °C, which were converted to zeta potential using the Smoluchowski equation. The dielectric constant of water medium is 78.54. The ζ-potential was measured using a U-shaped capillary cell that had gold electrodes (DTS1070). Prior to conducting the measurement, each U-shaped capillary cell was washed with ethanol, then rinsed with Milli-Q water several times, and next washed with the desired solution [62]. The ζ-potential of each DNAcol sample was measured in triplicate sequential auto-runs.

2.4. Porous medium

We used quartz sand as the porous medium, sieved to a 630–800 μm size. The sand was soaked in 10% (v:v) concentrated HNO_3 for approximately 24 h to remove the impurities (metal oxides) of the sand surface (adapted from Tian, et al. [63]). Then, the sand was repeatedly washed with Milli-Q water until the pH stabilized around neutral, and the electrical conductivity of the rinse water became ~2 μS cm^{-1}. Finally, the sand was oven dried at 105 °C for ~24 h.

2.5. Sand column experiments

A cylindrical acrylic column with an inner diameter of 2.7 cm and a height of 8 cm was filled with acid-washed sand. The columns were uniformly wet-packed using Milli-Q water, and the sand was added incrementally, while tapping the column. Two layers of mesh, one stainless-steel perforated layer and a small piece of nylon mesh, were placed at both ends of each column to ensure flow and tracer were distributed evenly throughout the column and to prevent clogging of tubing connected to the pump. The porosity of each sand column was determined in two ways: based on sand bulk density, assuming a sand grain density of 2.65 g cm^{-3}, and from curve fitting using HYDRUS-1D (see Section 2.9).

After packing the column, it was positioned vertically, and the inlet tubing of the column was connected to the pump. The flow was established in an upward direction. The column was flushed with Milli-Q water for more than 15 pore volumes, prior to conducting a tracer test with NaCl. For this NaCl tracer experiment, approximately 2.2 pore volumes (105 min) of NaCl was injected, followed by flushing with Milli-Q water. Then, the column was flushed with the desired solution for around 15 pore volumes to ensure the column was pre-equilibrated for the DNAcol experiment. The DNAcol experiments consisted of three phases: i) DNAcol injection phase (concentration of 1 mg L^{-1}) for 105 min (~2.2 pore volumes), ii) elution phase by injection of background (particle-free) solution for 180 min (~3.9 pore volumes), iii) transient porewater chemistry phase, by flushing the column with Milli-Q water for 180 min (~3.9 pore volumes). During the first two stages, DNAcol retention/attachment and detachment rate coefficients were determined. During the third stage (flushing with Milli-Q water) focus was on release of attached DNAcol. All column experiments were performed in duplicate, each time using cleaned and acid-washed sand. During the injection phase, the suspension was stirred continuously using a magnetic stirrer to ensure homogenous mixing. Over the time frame of DNAcol injection, 5–6 samples from the influent suspension were taken to determine DNA concentration and check stability of column influent (C_0).

Measured flow rates were 0.40 mL min^{-1} (± 0.02 mL min^{-1}), corresponding to a Darcy velocity of 0.07 cm min^{-1}, and were determined before and after each experiment by gravitationally measuring columns effluent. Column effluent was collected continuously with a sampling period of 5 min using a fraction collector (OMNICOLL, LAMBDA Laboratory Systems, Switzerland). For the NaCl tracer experiment, the Electrical Conductivity (EC) of the column effluent was measured as an indicator of salt concentration using a conductivity meter (GMH 3430 Greisinger, Germany). For DNAcol, collected samples were stored at 4 °C, and every other sample was analysed using quantitative polymerase chain reaction (qPCR).

2.6. qPCR analysis

Of each column effluent sample, a 20 μl subsample was taken and used for qPCR. The qPCR protocol was adapted from [53,57]; and [41]. Details regarding qPCR protocol, master mix, and calibration curve are presented in the supporting information (Section S1). In brief, the calibration curve was based on the known concentration of DNA in dilution series. In this study, the calibration curve was performed for each solution chemistry and primer batch specifically. Each calibration curve consisted of an 8-fold serial dilution ranging from 100 mg L^{-1} (D_2) to 0.00001 mg L^{-1} (D_9) (Supporting Information, Fig. S1). In addition to column effluent samples, to each qPCR run triplicate negative control samples (no template control (NTC)) containing ultra-pure water (DEPC-treated water), triplicate blank samples of column influent and effluent, and triplicate positive control samples in Milli-Q water, and in a desired background solution were added (Supporting Information, Fig. S2). The two types of positive controls contained a concentration of 10 mg L^{-1} (corresponding to D_3 in the calibration curve) of DNAcol in

Milli-Q water as a reference positive control, and the other one in the solution used. We did that to ensure there was no inhibition of qPCR signal, to check reproducibility of qPCR signal, to investigate and to compare the stability of DNAcol in various solution chemistries, and -in case of Milli-Q water to check long-term interexperimental stability of DNAcol (Supporting Information, Fig. S2).

2.7. Relative mass recovery

The relative mass recovery (M) of DNAcol under steady and transient porewater chemistry conditions was determined from:

$$M = \frac{\sum q\Delta t_i \frac{(C_i + C_{i+1})}{2}}{q t_{inj} C_0} \times 100 \quad (1)$$

Where q [cm^3 min] is the flow rate, Δt [min] is the time interval between analyzed column effluent samples, C_i [g cm^{-3}] is the measured sample concentration, t_{inj} [min] is the duration of injection phase of DNAcol (105 min), C_0 [g cm^{-3}] is the DNAcol injection concentration. For steady porewater chemistry conditions, the time interval was from the beginning of the experiment till 285 min, and then for transient porewater chemistry conditions it ended at 465 min.

The mass recovery of DNAcol remobilized during transient porewater chemistry conditions was calculated relative to the mass of retained DNAcol at the end of the steady porewater chemistry conditions. This we tentatively defined as $M_{transient}/M_{retained}$, whereby $M_{retained}$ was calculated as:

$$M_{retained} = M_{injection} - M_{steady} - M_{porewater} \quad (2)$$

$$M_{porewater} = (A.L.\theta).C_{porewater} \quad (3)$$

Where $M_{porewater}$ was defined as the mass in fluid phase at the end of the steady porewater chemistry conditions (i.e., end of flushing column with background solution), A [cm^2] is column surface, L [cm] is column length, θ [-] is porosity of the sand column, and $(A.L.\theta)$ is equal to the pore volume of each sand column, $C_{porewater}$ represents the average DNAcol concentration in three column samples: the last sample collected during steady porewater chemistry conditions, which was taken at the end of the elution phase, along with the analysed samples preceding and following it.

2.8. Sticking efficiency (α)

Based on colloid filtration theory [64], the deposition of colloidal particles in saturated porous media is governed by collector contact efficiency (η) and sticking efficiency (α). The single-collector contact efficiency (η_0) is associated with the frequency of colloids colliding with the grain surface and governed by diffusion, interception, and gravitational sedimentation [64,65]. The sticking efficiency (α) is the probability that the particles colliding within saturated porous media will attach to the grain surface (as a collector).

Typically, sticking efficiency (α) was obtained experimentally from breakthrough curve data (e.g. [65–69]):

$$\alpha = \frac{k_{att}}{\eta_0} \frac{2d_g}{3(1-\theta)v_p} \quad (4)$$

where k_{att} [cm^{-1}] is attachment or deposition rate coefficient, d_g [cm] is grain diameter, v_p [cm min^{-1}] is average pore water velocity, η_0 [-] is the single-collector contact efficiency. For determining η_0, we used the correlation equation proposed by Tufenkji and Elimelech (TE) [68] (Supporting Information, Section S3).

2.9. Modelling transport of DNAcol

We used the advection-dispersion-adsorption (see e.g. [70,71]) to model the macroscale transport of DNAcol:

$$\frac{\partial C}{\partial t} = \lambda_L v_p \frac{\partial^2 C}{\partial x^2} - v_p \frac{\partial C}{\partial x} - \frac{\rho_b}{\theta} \frac{\partial S}{\partial t} \quad (6)$$

$$\rho_b \frac{\partial S}{\partial t} = k_{att}\theta C - k_{det}\rho_b S \quad (7)$$

Where S [g g^{-1}] is the DNAcol on the solid phase, ρ_b [g cm^{-3}] is the dry bulk density, λ_L [cm] is the longitudinal dispersivity ($\lambda_L = D/v$, D: Dispersion coefficient), x [cm] is the travelled distance, and k_{att} and k_{det} [min^{-1}] are attachment and detachment rate coefficients, respectively.

The attachment rate coefficient (k_{att}) can be determined via inverse optimization of the advection-dispersion equation. In this study, we used HYDRUS-1D software [72] to estimate transport parameters. In this approach, first, porosity (θ) and dispersivity (λ_L) were determined from the normalized NaCl tracer experimental data (C/C_0) of each sand column. Then, with values of these two parameters fixed, attachment and detachment rate coefficients (k_{att} and k_{det}) were estimated. In HYDRUS, we employed the linear mode to determine attachment and detachment rate coefficients. We constrained the fitting during inverse modelling to a single set of parameters for attachment (k_{att}) and detachment (k_{det}). This approach implied that the model treated the attachment and retention as a lump in k_{att}, and detachment and reentrainment as k_{det}. Attachment refers to immobilization of colloids onto the surface of the collector through primary energy minimum, whereas retention refers to the temporary retention of colloids [73].

As mentioned above, we assigned to DNAcol particles the same dispersivity value as obtained for NaCl tracer in order to prevent overparameterization of the Hydrus model during the inverse modelling of DNAcol transport results. However, this approach could lead to the underestimation of particle dispersivity [73], since the value also depends on particle size [73]. Additionally, prior research showed that the rate of colloidal deposition can be greater when the flow direction is upward compared to downward [74]. We did not consider the effect of particle settling due to the upward flow direction, given the small size of DNAcol even though its specific density of around 2.2 g cm^{-3}. Therefore, we expected a negligible effect on settling and deposition based on the flow direction.

2.10. DLVO interaction energy profile

Derjaguin-Landau-Verwey-Overbeek (DLVO) was used to qualitatively explain the column breakthrough results [99,100]. Total interaction energy as a function of separation distance was defined based on the sum of electrical double-layer (EDL) and van der Waals (vdW) energies (details in Supporting Information, Section S4).

3. Results

3.1. Characterization of DNAcol

The ζ-potentials of DNAcol were negative for all tested conditions (Table 1). Average values varied from ~ −50 mV to −17 mV, in the presence of DOC 20 mg-C L^{-1} to ionic strength of 10 mM. The measured ζ-potential of DNAcol in water was determined to be −33 mV. However, in the presence of DOC at concentrations of 5 and 20 mg-C L^{-1}, the ζ-potential became more negative, with average values of approximately −42 mV and −50 mV, respectively. Conversely, an opposing trend was observed when $CaCl_2$ was added, and it became –18 to −19 mV. This trend suggested that the presence of $CaCl_2$, lead to a decrease in the absolute value of the ζ-potential. This could be attributed to shielding of the surface charge of the DNAcol, and compression of the double layer [5,15]. Conversely, in the presence of DOC at concentrations of 5 and 20 mg-C L^{-1}, the ζ-potential became more negative. This shift was possibly due to the adsorption of negatively charged organic

matter onto the DNAcol surface. In order to assess colloidal stability of the DNAcol suspension, the ζ-potential was measured after 120 min. Changes in ζ-potential values over time were negligible. Average hydrodynamic diameter, d_h, of DNAcol in Milli-Q water was 311 nm, with a polydispersity index (PDI) of 0.24 (Table 1). The average d_h diameter of DNAcol for the tested conditions varied from 296 to 311 nm.

3.2. Column breakthrough curves

3.2.1. Steady porewater chemistry conditions

Breakthrough curves of NaCl reached C_{max}/C_0 values of 1 with a characteristic S-shaped rising limb (Fig. S5) from which dispersivity and porosity of the sand column could be determined. Also, the start of the NaCl rising limb and DNAcol breakthrough curves coincided from which we concluded that pore size exclusion effects in our columns did not play an important role (Fig. S5).

Under steady porewater chemistry conditions, the breakthrough of DNAcol in Milli-Q water reached a plateau concentration ($C_{plateau}/C_0$) of 0.78–0.85, where $C_{plateau}$ represented the average concentration between 65 and 105 min. The mass recovery of DNAcol in this experiment was on average 81% (Table 2). By adding $CaCl_2$ with ionic strength of 1 mM the plateau phase of the breakthrough curves substantially decreased to 0.02 ($C_{plateau}/C_0$), and only ~2% of injected particles mass was recovered from the sand column (Fig. 1B, Table 2). This outcome pointed towards a high attachment or retention of DNAcol within the sand column. The tailing of the breakthrough curves in this experiment, (Fig. 1B), exhibited a sharp decline, indicative of negligible detachment and/or reentrainment. In the case of 10 mM $CaCl_2$ solution, a similar low plateau phase was observed, accompanied by a rapid decrease in the declining limb. The relative mass recovery of DNAcol in this case was only about 1% (Fig. 1C; Table 2).

In the presence of 5 mg-C L^{-1} DOC, the plateau concentration ($C_{plateau}/C_0$) ranged approximately from 0.83 to 0.89, suggesting a low attachment rate of DNAcol. In this case, the tailing of the breakthrough curve gradually decreased. The extended declining limb of the breakthrough curve indicated significant re-entrainment. Under this condition, the relative mass recovery of DNAcol was ~85% (Fig. 1D; Table 2). Upon increasing of porewater's ionic strength to 1 mM $CaCl_2$, while the concentration of organic matter was kept at 5 mg-C L^{-1} DOC, the plateau phase decreased to 0.45–0.52. This reduction highlighted a higher attachment or retention rate of DNAcol within the sand column. Similarly to the previous case (Fig. 1D), the declining limb exhibited a gradual decrease, indicating re-entrainment. However, the mass recovery of DNAcol was only 49% (Fig. 1E; Table 2). Upon further increasing the ionic strength to 10 mM $CaCl_2$ while maintaining the concentration of 5 mg-C L^{-1} DOC, the mass recovery of DNAcol decreased even further to ~12% (Fig. 1F; Table 2).

In two experiments conducted with 20 mg-C L^{-1} DOC, both in the absence and presence of 1 mM $CaCl_2$ ionic strength (Fig. 1G-H), the breakthrough curves reached their highest plateau values, approximately 0.9. Similar to the previous conditions with a lower DOC concentration, both cases exhibited breakthrough curves with extended tails, followed by a gradual decline (Fig. 1G-H). The DNAcol mass recovery exceeded 90% in these experiments (Table 2). However, when 20 mg-C L^{-1} DOC was present along with an elevated ionic strength of 10 mM $CaCl_2$, the plateau of the breakthrough curve significantly decreased to a range of 0.14–0.28 (Fig. 1I). This pattern demonstrated an increased attachment or retention rate due to the higher ionic strength. Correspondingly, the mass recovery decreased to a range of 14–25% (Table 2).

In the experiment conducted at an ionic strength of 1 mM $CaCl_2$ with 20 mg-C L^{-1} DOC, we observed that the mass recovery of DNAcol exceeded 100%, which was likely associated with sensitivity of qPCR in detection of DNA. To evaluate variation between subsamples, for some of the experiments, each collected sample was analysed twice, with two different qPCR runs. The variation between these sub-samples was depicted as shaded areas in Fig. S6.

3.2.2. Transient porewater chemistry conditions

After the elution phase of DNAcol (i.e., injection of free-particles solution phase), the columns were flushed with Milli-Q water to induce remobilization of colloids. This we called transient porewater chemistry conditions. In all cases, (Fig. 1B-I; filled symbols), we observed a second peak upon flushing the column with Milli-Q water. It was evident from the breakthrough curves (Fig. 1B-I), the magnitude of the peak differed for the experiments.

Initially, we noticed that $M_{transient}/M_{injection}$ was always lower than 22% (Table 2). These results indicated that the fraction of remobilized DNAcol was relatively small. Additionally, in experiments conducted with the ionic strength $\leq$ 1 mM $CaCl_2$ the second peak (i.e., transient peak) was low. In contrast, for experiments with ionic strength 10 mM $CaCl_2$ the transient peak appeared rather sharp and more noticeable. In detail, during transient porewater chemistry conditions, in the cases of $\leq$ 1 mM $CaCl_2$ the relative mass recovery ($M_{transient}/M_{injection}$) of DNAcol was around 1%, and for the three cases with an ionic strength of 10 mM $CaCl_2$ the relative mass recovery ($M_{transient}/M_{injection.}$) of DNAcol ranged between ~7–21% (Table 2; Fig. 2A). When comparing the breakthrough curves DNAcol for ionic strength 1 and 10 mM $CaCl_2$ conditions, under steady porewater chemistry conditions, the obtained mass recovery was 1% and 2%, respectively. However, under transient porewater chemistry conditions, the relative mass recovery averaged around 0.26% and 9% for ionic strength 1 mM and 10 mM conditions, respectively (Table 2). The difference in the magnitude of relative mass recovery indicated distinct attachment and release patterns. Additionally, in the experiment with ionic strength of 10 mM $CaCl_2$, the relative mass recovery during transient porewater chemistry conditions was ~7 times higher than relative mass recovery during steady porewater chemistry conditions. In the experiment of 10 mM $CaCl_2$ with 5 mg-C L^{-1} DOC the relative mass recovery ($M_{transient}/M_{injection}$) was ~19%, which then reduced to ~12% in presence of 20 mg-C L^{-1} DOC (Table 2).

Fig. 2B shows also the mass recovery of DNAcol remobilized during transient porewater chemistry conditions relative to the mass of retained DNAcol at the end of the steady porewater chemistry conditions. Fig. 2B shows $M_{transient}/M_{retained}$ values were lowest for ionic strength of 1 mM $CaCl_2$. However, care should be taken in interpreting the experiments in

Table 2
Summary of relative mass recovery of DNAcol under steady porewater chemistry conditions ($M_{steady}/M_{injection}$), transient porewater chemistry conditions ($M_{transient}/M_{injection}$), and total mass recovery (M_{total}). C_{max}/C_0 is the maximum relative concentration.

Column Experiment	Solution	C_{max}/C_0 [-]	$M_{steady}/M_{injection}$ [%]	$M_{transient}/M_{injection}$ [%]	M_{total} [%]
A1	Milli-Q water	0.8	76.96	-	76.96
A2	Milli-Q water	0.9	85.20	-	85.20
B1	I1	0.02	1.62	0.29	1.91
B2	I1	0.05	2.07	0.24	2.30
C1	I10	0.02	1.59	11.31	12.90
C2	I10	0.04	1.28	7.54	8.82
D1	DOC5	1.0	91.29	1.06	92.35
D2	DOC5	0.9	77.98	1.15	79.13
E1	DOC5-I1	0.6	46.85	0.81	47.67
E2	DOC5-I1	0.7	50.66	0.99	51.65
F1	DOC5-I10	0.2	13.31	17.21	30.52
F2	DOC5-I10	0.1	11.64	21.31	32.95
G1	DOC20	1.0	91.20	0.97	92.17
G2	DOC20	1.0	93.50	1.12	94.62
H1	DOC20-I1	1.0	88.66	0.88	89.55
H2	DOC20-I1	2.9	123.33	0.97	124.30
I1	DOC20-I10	0.3	24.63	10.18	34.82
I2	DOC20-I10	0.2	14.38	13.29	27.68

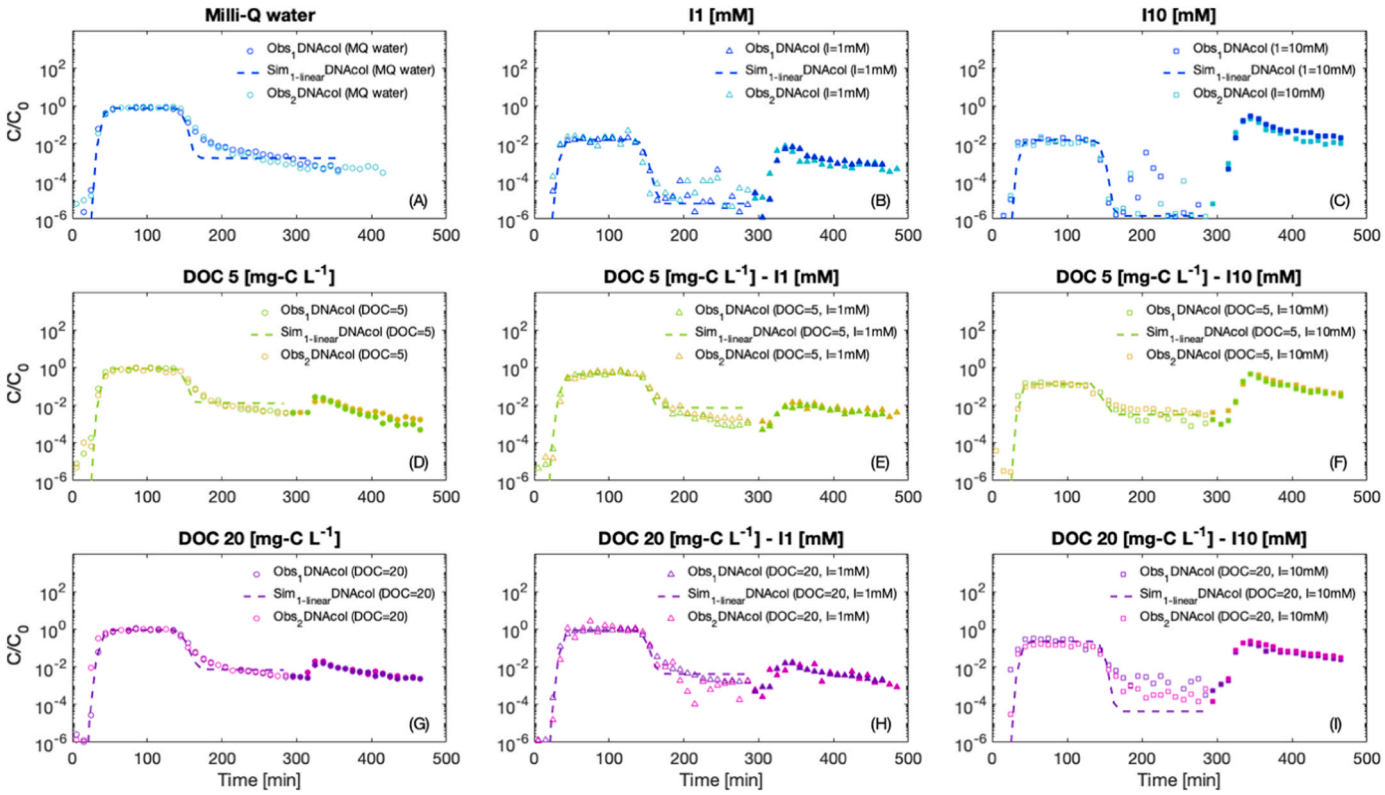

Fig. 1. DNAcol breakthrough curves (symbols) and HYDRUS model fits (dashed lines). Background solutions: (A) Milli-Q water, (B) 1 mM $CaCl_2$, (C) 10 mM $CaCl_2$, (D) DOC 5 mg-C L^{-1}, (E) DOC 5 mg-C L^{-1} with 1 mM $CaCl_2$, (F) DOC 5 mg-C L^{-1} with 10 mM $CaCl_2$, (G) DOC 20 mg-C L^{-1}, (H) DOC 20 mg-C L^{-1} with 1 mM $CaCl_2$, (I) DOC 20 mg-C L^{-1} with 10 mM $CaCl_2$. Hollow symbols represent DNAcol concentration during steady porewater chemistry conditions, and filled symbols represent transient porewater chemistry conditions.

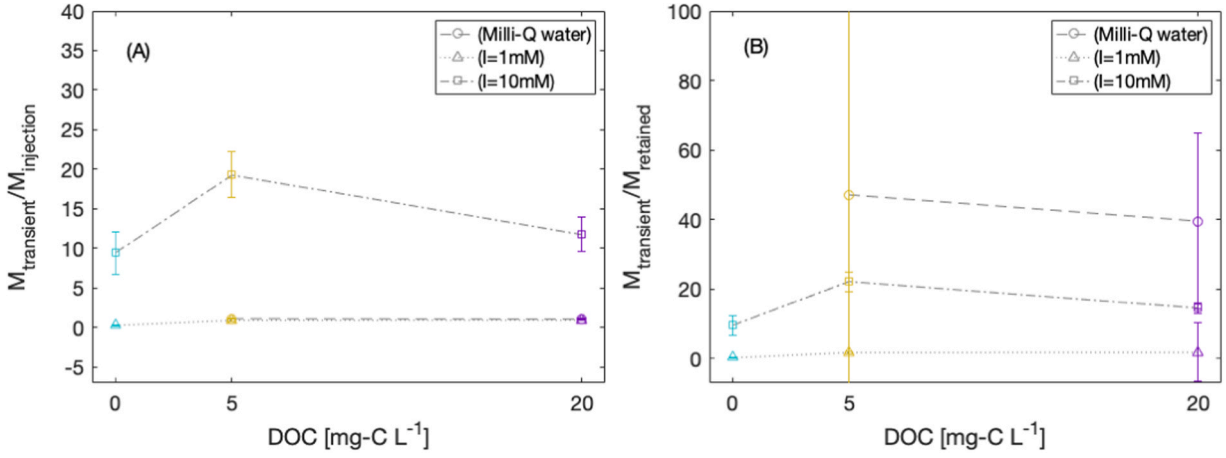

Fig. 2. (A) Ratios determined from mass recoveries during transient porewater chemistry conditions to mass injection as a function of DOC concentration ($M_{transient}/M_{injection}$), and (B) Ratios determined from mass recoveries during transient porewater chemistry conditions to mass retained in the column ($M_{transient}/M_{retained}$).

case of experiments 5, 20 mg-C L^{-1} DOC, and 20 mg-C L^{-1} DOC with ionic strength 1 mM as there was not much DNAcol mass retained in the column before flushing the column with Milli-Q water (Table 2: steady porewater chemistry conditions mass recovery on average ~85–106%). Note that, in a few cases of those experiments, the relative concentration of the samples was (C/C_0) slightly above 1.

3.2.3. *HYDRUS-1D curve fitting and sticking efficiencies*

HYDRUS-1D was used to fit a model through the breakthrough data and determine attachment and detachment rate coefficients (Fig. 1, dashed lines; Table 3). The overall values of the goodness of fits (R^2) ranged from 0.77 to 0.99. In general, attachment rate coefficients decreased as a function of DOC and increased as a function of ionic strength ($CaCl_2$) (Table 3). Furthermore, detachment rate coefficients decreased upon increase of ionic strength ($CaCl_2$), while an increase in DOC in most cases led to a higher detachment rate coefficient (Table 3). The calculated sticking efficiency (α) for Milli-Q water and porewater containing DOC was ~10^{-2} (Table 3). However, for porewater containing 1 or 10 mM of $CaCl_2$, it increased to 1, which indicated more favourable attachment conditions. In case both $CaCl_2$ and DOC were present, the order of magnitude of α was ~10^{-1}-10^{-2} (Table 3).

Table 3
Estimated attachment-detachment rate coefficients from HYDRUS and sticking efficiency values (α). For the single-collector contact efficiency (η_0) of the sand-column system, the value was 0.04. Sticking efficiencies were calculated using d_p = 280 [nm], d_g= 0.715 [mm], Hamaker constant: H= 0.7 × 10^{-20} [J], ρ_p = 2200 [kg m^{-3}].

Solution	Hydrus		α
	k_{att} [min^{-1}]	k_{det} [min^{-1}]	Eq. 4
Milli-Q water	6.65 × 10^{-3}	0.08 × 10^{-3}	0.07
I1	100.39 × 10^{-3}	0.002 × 10^{-3}	1.07
I10	103.39 × 10^{-3}	0.0002 × 10^{-3}	1.05
DOC5	3.52 × 10^{-3}	1.13 × 10^{-3}	0.04
DOC5-I1	19.58 × 10^{-3}	0.2 × 10^{-3}	0.20
DOC5-I10	48.72 × 10^{-3}	0.11 × 10^{-3}	0.49
DOC20	2.59 × 10^{-3}	0.76 × 10^{-3}	0.03
DOC20-I1	3.32 × 10^{-3}	0.35 × 10^{-3}	0.03
DOC20-I10	36.42 × 10^{-3}	0.003 × 10^{-3}	0.37

3.2.4. Interaction energy profiles

Upon increase of ionic strength as function of $CaCl_2$ concentration, the height of the energy barrier decreased and the depth of the secondary minimum increased (Fig. S3, Fig. S4). This explained the higher attachment/retention rates at higher ionic strength. For example, for the case of DOC 5 mg-C L^{-1}, the height of the potential energy barrier was 465k_BT, while for the case of DOC 5 mg-C L^{-1} with ionic strength 10 mM, the height of the energy barrier decreased to 51k_BT, due to the diffuse double layer compressed. In addition, upon increase in ionic strength, the depth of the secondary minimum became pronounced. For the experiment of DOC 5 mg-C L^{-1} with ionic strength 10 mM, the depth of the secondary minimum was –0.358k_BT.

Upon increase in DOC concentration, DNAcol became more negative, leading to higher electrostatic repulsion between DNAcol. However, the DLVO profile could not capture the low attachment rate of DNAcol in the presence of DOC 20 mg-C L^{-1} with ionic strength 1 mM. In all cases, the deep primary energy well remained, mainly because ζ-potentials of DNAcol varied only slightly, while the mass recovery increased substantially. This observation highlighted the importance of steric repulsion in reducing the deposition rate of the DNAcol. In our study, we did not consider the effect of short-range repulsive forces and steric repulsion. The omission of steric repulsion was due to our inability to accurately define the thickness of the adsorbed NOM layer, the distance between the chains on the surface and adsorbed mass, which is crucial in the context of steric repulsion.

4. Discussion

We started by examining the experiment with DNAcol suspended in Milli-Q water, without the adding of NOM and $CaCl_2$. In this experiment, we observed that the breakthrough curves reached the plateau phase with a ($C_{plateau}/C_0$) value of ~0.8, Fig. 1A. The relative mass recovery of less than 100% could be attributed to the trapping of some of the particles in the dead-end pores [75], surface roughness, and the presence of patchwise macroscale and nanoscale heterogeneity on the surface of the grain, which could act as attachment sites [67].

In the experiments involving only Ca^{2+} at ionic strengths of 1 and 10 mM, Fig. 1B and C, the plateau phase of the breakthrough curves drastically decreased, with a 2 log removal. The tails of both breakthrough curves also exhibited a sharp decline, and negligible tailing. From the literature, we understood that the presence of Ca^{2+} could lead to an increase in attachment. This increase could be attributed to double layer compression, charge screening [15], or Ca-bridging between the silica surface of the sand and DNAcol, or a combination of factors. The calcium bridging between the silica surfaces and anionic surfactant is well known in the literature (e.g. [76]). We initially anticipated a higher attachment rate for the experiment with ionic strength of 10 mM in comparison to the 1 mM experiment. However, the increase in attachment rate was minimal. The sticking efficiencies belonging to these two experiments were approximately around 1, indicating favourable or nearly favourable attachment conditions [77]. Based on these results, we expected that the majority of DNAcol colliding with the sand grain surface could also attach to it. However, despite this expectation, the DLVO profile indicated the presence of a potential barrier. Recent studies have reported the limitation of the mean-field DLVO theory in predicting attachment when potential energy barriers are present [50,51,78–81]. For DLVO calculations, we assumed a smooth particle surface with uniform size and charge. This approximation may lead to overestimating unfavourable conditions. Additionally, we assumed the ζ-potential of the sand grains were similar to DNAcol. Beyond these assumptions, a limitation of the DLVO likely was related to the presence of heterogeneity, like charge and roughness on the surfaces [67,77,82–85]. The presence of macro and nano scale heterogeneity could play a role in mitigating the repulsive energy barrier. In this direction, recently, mechanistic approaches were presented that aim to explain both attachment and detachment from primary energy minima, even under unfavourable conditions [51,82].

Upon examining the experiments involving only NOM (Exps. D and G), we expected a higher level of electrostatic repulsion and the presence of steric hindrance, leading to a lower rate of DNAcol attachment. Additionally, NOM was anticipated to have a “masking-effect” [29], reducing surface heterogeneity, and also enhancing transport of colloidal matter [29,86,87]. The adsorption of NOM onto both sand grains and suspended colloidal particles surfaces led to an increase in electrostatic repulsion force due to the increase in the ζ-potential values [19,88,89]. This increase in the negative charge was observed within just 5 min upon adding DNAcol to the solutions. In these two experiments, based on the breakthrough curves results, it became clear that the plateau values of the breakthrough curves reached higher levels, indicating lower DNAcol attachment or retention. The estimated k_{att}, and k_{det} values further confirmed this trend, with k_{att} being lower and k_{det} being higher compared to the experiments of DNAcol in Milli-Q water. The mass recovery of the experiments conducted with Milli-Q water was approximately 81% (Exp. A), and the mass recoveries increased to 85% and then to around 92% for the experiments involving 5 and 20 mg-C L^{-1} DOC, respectively (Exps. D and G). This indicated that steric hindrance played a role to a certain extent, which was extensively described in the literature [13,15,19,21,27,30,90].

As mentioned earlier, ionic strength had a major effect on transport of DNAcol, leading to a significant increase in the attachment rate. However, DOC had an opposite effect on attachment rate. When both Ca^{2+} and DOC were present in the solution (Exps. E, F, H, and I), then we think the [Ca^{2+}]/DOC ratio started playing a role. In these combined experiments, Ca^{2+} could not only bind to the two silica surfaces present in the system but also to DOC (e.g. [91]). For the lowest [Ca^{2+}]/DOC ratio, where the ionic strength was 1 mM and DOC was 20 mg-C L^{-1} (Exp. H), we observed that the plateau ($C_{plateau}/C_0$) of the breakthrough curves approached values close 0.8–1. Remarkably, in this experiment, the mass recovery increased massively compared to conditions with the same ionic strength but without NOM (no DOC). The associated sticking efficiency for this experiment was 0.03. These results showed that the presence of 20 mg-C L^{-1} of DOC effectively outcompete DNAcol attachment, which was an interesting finding in the framework of the DNAcol application for tracer transport studies or when considering the ecotoxicity of colloids. For the second lowest [Ca^{2+}]/DOC ratio (ionic strength of 1 mM with DOC of 5 mg-C L^{-1}), the k_{att} value was one order of magnitude larger than in the previous case, that contained a higher DOC concentration. In this experiment, the plateau of the breakthrough curves reached approximately 0.48, indicating a higher rate of attachment within the sand column. Finally, for the ionic strength of 10 mM experiments with DOC of 5 and 20 mg-C L^{-1}, the k_{att} values increased further when compared to the conditions with ionic strength of 1 mM. In these two experiments, the mass recoveries increased from 1% (no DOC; Exp. C) to approximately 12–20%, (Exps. F, and I), respectively. The

most plausible explanation for this observation could be attributed to inter-molecular cation bridging or complexation facilitated by the presence of Ca^{2+} ion, between the negatively charged surfaces of NOM and the sand grains [21]. Furthermore, as ionic strength increases the zone of colloid-collector interaction shrinks [50], potentially leading to a higher attachment rate [51]. We expected the thickness of the adsorbed organic matter layer on DNAcol would be affected by increasing ionic strength. That meant that repulsion between the nearest adsorbed macromolecules was reduced to some extent due to a decrease in negative charge [36]. Consequently, this could result in a denser and more compacted configuration of the adsorbed organic layer [36,92]. We initially attempted to indirectly determine the thickness of the adsorbed NOM layer on DNAcol, by comparing the hydrodynamic diameters of DNAcol in the absence and presence of organic matter. However, this approach was impractical due to hydrodynamic diameter being a rather coarse measurement of true particle diameter, coupled with the broad size distribution of the hydrodynamic diameter of DNAcol exceeding the expected thickness of the adsorbed layer.

Under transient porewater chemistry conditions, we observed the release of DNAcol upon flushing with Milli-Q water. Such remobilization phenomenon was reported by other researchers in relation to various types of colloidal matter (e.g. [9,13,27,41,42,44,45,93]. The remobilization can provide evidence to enhance our understanding to what extent the colloidal matter was attached reversibly or irreversibly within the sand column. Under transient porewater chemistry conditions, comparing the two experiments with ionic strength of 1 mM and 10 mM revealed distinct differences in the release of DNAcol upon flushing the column with Milli-Q water. While the deposition rates of DNAcol in ionic strength of 1 and 10 mM under steady porewater chemistry conditions were quite similar, the remobilization rate of retained or attached particles significantly differed under transient porewater chemistry conditions. Specifically, the release of DNAcol deposited at an ionic strength of 10 mM was significantly higher compared to those at 1 mM (see Fig. 1 and Fig. S6 in Support information).

As the study of Nocito-Gobel and Tobiason [94] indicated, the rate of particle release resulting from reducing in ionic strength might be influenced by various factors, such as the magnitude of the ionic strength change, the final ionic strength value, as well as the type and the quantity of previously deposited particles. This study also observed the highest rate of release for particles deposited in the 10 mM experiment [94]. Obviously, for the two experiments with 1 mM and 10 mM ionic strength, we could assume that the final value of the change in ionic strength was similar, as the columns were flushed around 3 PVs with Milli-Q water. Furthermore, the mass recovery values calculated under steady porewater chemistry conditions were 2% and 1% for ionic strength of 1 mM and 10 mM, respectively. Therefore, we could reasonably assume that the amount of the previously deposited particles in both cases were rather similar. Here, the results highlighted the critical role of the magnitude of change in ionic strength in release rate, during transient porewater chemistry conditions. For example, Franchi and O'Melia [13] highlighted that during transient conditions, when the column was rinsed with lower ionic strength, a sharp peak appeared, and the peak magnitude increasing with the change in ionic strength during injection phase. Other studies have indicated that significant remobilization of colloidal particles can occur when the reduction in ionic strength reaches a critical concentration [42,95]. Our results also showed higher DNAcol release rate upon flushing the column with Milli-Q water for experiments conducted at higher ionic strength (Exps. C, F, and I) than experiments conducted at the lower ionic strength.

Even though the experimental conditions were theoretically performed under unfavourable conditions, it remained unclear what could be the main reason behind the remobilization of DNAcol upon change in pore water chemistry. It is important to emphasize that although the column experiment results improved our understanding of DNAcol transport behaviour, and the rate of removal, more work is necessary to accurately describe the underlying mechanisms involved in the attachment, retention, and remobilization. The one explanation for the higher rate of particles remobilization at 10 mM $CaCl_2$ during the transient porewater chemistry conditions could be linked to the depth and positioning of the secondary minimum [6]. Commonly, the release of particles is associated with a secondary energy minimum in DLVO theory [13,96]. The DLVO profile indicated under 10 mM ionic strength conditions, the secondary minimum was deeper and situated closer to the surface of the sand grains. However, upon a closer examination of the DLVO profile, it became apparent that the secondary minimum was quite shallow in cases of 10 mM ionic strength.

The other possible mechanism contributing to the release of DNAcol upon flushing with Milli-Q water, could be detachment of particles from the primary energy. As previously mentioned, the presence of nanoscale heterogeneity on the surface can diminish or even eliminate the repulsive barrier, under unfavourable conditions, thereby leading to attachment in the primary energy well [51]. This nanoscale heterogeneity in surface charge could also account for particle detachment under unfavourable conditions with respect to ionic strength reduction [82,97]. Moreover, the presence of nanoscale heterogeneity, such as surface physical asperities, might have contributed to the retention of particles [98].

It is important to note that in our experiments conducted with 1 mM and 10 mM ionic strength, only a small fraction of the attached or retained DNAcol were released upon reducing the ionic strength. This observation suggested that in these two cases, the majority of the DNAcol (approximately 98–90%) was strongly bound to the sand grains and remained unreleased. It could be tempting to conclude that Ca-bridging between the sand and DNAcol yielded binding strengths, that could not be broken by the decrease in solution ionic strength.

5. Conclusions

The experimental results indicated that ionic strength and organic matter had opposite effects on the overall transport and attachment rate of DNAcol. As a result, the transport behaviour of DNAcol exhibited substantial variability across the range of tested conditions. Consequently, if we aim for the application of DNAcol as a tracer for mass balance, its applicability may fail due to its high sensitivity to environmental conditions.

So, in summary the results of this study demonstrated that:

- The concentration of DOC in the aqueous system can play a crucial role in the transport and fate of DNAcol.
- The calculations of sticking efficiency indicated that in the presence of organic matter the probability of DNAcol attachment decreased significantly.
- Attachment of DNAcol was regulated by the $[Ca^{2+}]$/DOC ratio, whereby attachment was low at low ratios and increased when $[Ca^{2+}]$/DOC ratio increased. There was a range of $[Ca^{2+}]$/DOC ratios, whereby the attachment of DNAcol to the sand grains was negligible.
- The remobilization of DNAcol was more significant under transient porewater chemistry conditions with 10 mM ionic strength compared to 1 mM $CaCl_2$. These findings emphasize the importance of evaluating the impact of transient porewater chemistry conditions on the potential risk of colloidal transport.

CRediT authorship contribution statement

Bahareh Kianfar: Conceptualization, Methodology, Investigation, Visualization, Writing – original draft, Writing – review & editing. **S. Majid Hassanizadeh:** Methodology, Supervision, Writing – review & editing. **Ahmed Abdelrady:** Conceptualization, Methodology, Writing – review & editing. **Thom A. Bogaard:** Funding acquisition, Conceptualization, Resources, Writing – review & editing. **Jan Willem Foppen:** Conceptualization, Funding acquisition, Supervision, Resources,

Writing – original draft, Writing – review & editing.

Declaration of Generative AI and AI-assisted technologies in the writing process

During the preparation of this work, the author used ChatGPT in order to improve readability and language. After using this tool/service, the authors reviewed and edited the content as needed and take full responsibility for the content of the publication.

Declaration of Competing Interest

The authors declare that they have no known competing financial interests or personal relationships that could have appeared to influence the work reported in this paper.

Data Availability

Data will be made available on request.

Acknowledgments

We are thankful to prof. Robert N. Grass, dr. Gediminas Mekutis, and dr. Julian Koch (Department of Chemistry and Applied Biosciences ETH Zurich), for kindly providing DNAcol. We are very thankful to Nasir Mangel for kindly providing humic acid stock. We thank Bright Namata for assisting with qPCR analyses, and Ferdi Battes (IHE Delft) for zeta measurement assistance. Also, we thank dr. Mohsen Mirzaie Yegane (TU Delft) for insightful discussions. The research was supported by the Netherlands Organization for Scientific Research (NWO), TTW grant 14514 WaterTagging. SMH acknowledges support by the Stuttgart Center for Simulation Science (SimTech). We would like to thank TU Delft Waterlab and IHE-Delft laboratory staff, and IHE-Delft for laboratory support and access to conduct this research.

Appendix A. Supporting information

Supplementary data associated with this article can be found in the online version at doi:10.1016/j.colsurfa.2023.132476.

References

[1] J. McCarthy, J. Zachara, ES&T features: subsurface transport of contaminants, Environ. Sci. Technol. vol. 23 (5) (1989) 496–502.
[2] M.R. Wiesner, et al., Decreasing uncertainties in assessing environmental exposure, risk, and ecological implications of nanomaterials, ed: ACS Publ. (2009).
[3] M.R. Wiesner, G.V. Lowry, P. Alvarez, D. Dionysiou, P. Biswas, Assessing the risks of manufactured nanomaterials, ACS Publ. (2006).
[4] A.R. Petosa, D.P. Jaisi, I.R. Quevedo, M. Elimelech, N. Tufenkji, Aggregation and deposition of engineered nanomaterials in aquatic environments: role of physicochemical interactions, Environ. Sci. Technol. vol. 44 (17) (2010) 6532–6549.
[5] S. Torkzaban, S. Hassanizadeh, J. Schijven, H. De Bruin, A. de Roda Husman, Virus transport in saturated and unsaturated sand columns, Vadose Zone J. vol. 5 (3) (2006) 877–885.
[6] G. Chen, X. Liu, C. Su, Distinct effects of humic acid on transport and retention of TiO2 rutile nanoparticles in saturated sand columns, Environ. Sci. Technol. vol. 46 (13) (2012) 7142–7150.
[7] P. Han, X. Wang, L. Cai, M. Tong, H. Kim, Transport and retention behaviors of titanium dioxide nanoparticles in iron oxide-coated quartz sand: effects of pH, ionic strength, and humic acid, Colloids Surf. A: Physicochem. Eng. Asp. vol. 454 (2014) 119–127.
[8] P.N. Mitropoulou, V.I. Syngouna, C.V. Chrysikopoulos, Transport of colloids in unsaturated packed columns: Role of ionic strength and sand grain size, Chem. Eng. J. vol. 232 (2013) 237–248.
[9] G. Sadeghi, T. Behrends, J.F. Schijven, S.M. Hassanizadeh, Effect of dissolved calcium on the removal of bacteriophage PRD1 during soil passage: the role of double-layer interactions, J. Contam. Hydrol. vol. 144 (1) (2013) 78–87.
[10] J.W. Foppen, Y. Liem, J. Schijven, Effect of humic acid on the attachment of Escherichia coli in columns of goethite-coated sand, Water Res. vol. 42 (1–2) (2008) 211–219.
[11] A.R. Petosa, S.J. Brennan, F. Rajput, N. Tufenkji, Transport of two metal oxide nanoparticles in saturated granular porous media: role of water chemistry and particle coating, Water Res. vol. 46 (4) (2012) 1273–1285.
[12] B. Espinasse, E.M. Hotze, M.R. Wiesner, Transport and retention of colloidal aggregates of C60 in porous media: effects of organic macromolecules, ionic composition, and preparation method, Environ. Sci. Technol. vol. 41 (21) (2007) 7396–7402.
[13] A. Franchi, C.R. O'Melia, Effects of natural organic matter and solution chemistry on the deposition and reentrainment of colloids in porous media, Environ. Sci. Technol. vol. 37 (6) (2003) 1122–1129.
[14] L. Goswami, et al., Engineered nano particles: nature, behavior, and effect on the environment, J. Environ. Manag. vol. 196 (2017) 297–315.
[15] V.L. Morales, et al., Impact of dissolved organic matter on colloid transport in the vadose zone: deterministic approximation of transport deposition coefficients from polymeric coating characteristics, Water Res. vol. 45 (4) (2011) 1691–1701.
[16] W. Zhang, U.-S. Rattanaudompol, H. Li, D. Bouchard, Effects of humic and fulvic acids on aggregation of aqu/nC60 nanoparticles, Water Res. vol. 47 (5) (2013) 1793–1802.
[17] H. Ohshima, Electrophoretic mobility of soft particles, J. Colloid Interface Sci. vol. 163 (2) (1994) 474–483.
[18] G.V. Lowry, et al., Guidance to improve the scientific value of zeta-potential measurements in nanoEHS, Environ. Sci.: Nano vol. 3 (5) (2016) 953–965.
[19] J.E. Patino, T.L. Kuhl, V.L. Morales, Direct measurements of the forces between silver and mica in humic substance-rich solutions, Environ. Sci. Technol. vol. 54 (23) (2020) 15076–15085.
[20] L. Xu, M. Xu, R. Wang, Y. Yin, I. Lynch, S. Liu, The crucial role of environmental coronas in determining the biological effects of engineered nanomaterials, Small vol. 16 (36) (2020), 2003691.
[21] K.L. Chen, M. Elimelech, Influence of humic acid on the aggregation kinetics of fullerene (C60) nanoparticles in monovalent and divalent electrolyte solutions, J. Colloid Interface Sci. vol. 309 (1) (2007) 126–134.
[22] N.B. Saleh, L.D. Pfefferle, M. Elimelech, Aggregation kinetics of multiwalled carbon nanotubes in aquatic systems: measurements and environmental implications, Environ. Sci. Technol. vol. 42 (21) (2008) 7963–7969.
[23] Y. Zhang, Y. Chen, P. Westerhoff, J. Crittenden, Impact of natural organic matter and divalent cations on the stability of aqueous nanoparticles, Water Res. vol. 43 (17) (2009) 4249–4257.
[24] G.R. Aiken, H. Hsu-Kim, J.N. Ryan, Influence of dissolved organic matter on the environmental fate of metals, nanoparticles, and colloids, ACS Publ. (2011).
[25] A. Amirbahman, T.M. Olson, The role of surface conformations in the deposition kinetics of humic matter-coated colloids in porous media, Colloids Surf. A: Physicochem. Eng. Asp. vol. 95 (2–3) (1995) 249–259.
[26] R. Grillo, A.H. Rosa, L.F. Fraceto, Engineered nanoparticles and organic matter: a review of the state-of-the-art, Chemosphere vol. 119 (2015) 608–619.
[27] D.P. Jaisi, N.B. Saleh, R.E. Blake, M. Elimelech, Transport of single-walled carbon nanotubes in porous media: filtration mechanisms and reversibility, Environ. Sci. Technol. vol. 42 (22) (2008) 8317–8323.
[28] S.M. Louie, E.R. Spielman-Sun, M.J. Small, R.D. Tilton, G.V. Lowry, Correlation of the physicochemical properties of natural organic matter samples from different sources to their effects on gold nanoparticle aggregation in monovalent electrolyte, Environ. Sci. Technol. vol. 49 (4) (2015) 2188–2198.
[29] A.J. Pelley, N. Tufenkji, Effect of particle size and natural organic matter on the migration of nano-and microscale latex particles in saturated porous media, J. Colloid Interface Sci. vol. 321 (1) (2008) 74–83.
[30] T. Phenrat, J.E. Song, C.M. Cisneros, D.P. Schoenfelder, R.D. Tilton, G.V. Lowry, Estimating attachment of nano-and submicrometer-particles coated with organic macromolecules in porous media: development of an empirical model, Environ. Sci. Technol. vol. 44 (12) (2010) 4531–4538.
[31] F. Zhang, Z. Wang, S. Wang, H. Fang, D. Wang, Aquatic behavior and toxicity of polystyrene nanoplastic particles with different functional groups: complex roles of pH, dissolved organic carbon and divalent cations, Chemosphere vol. 228 (2019) 195–203.
[32] M. Zhang, et al., Effect of humic acid on the sedimentation and transport of nanoparticles silica in water-saturated porous media, J. Soils Sediment. vol. 20 (2) (2020) 911–920.
[33] Z. Li, K. Greden, P.J. Alvarez, K.B. Gregory, G.V. Lowry, Adsorbed polymer and NOM limits adhesion and toxicity of nano scale zerovalent iron to E. coli, Environ. Sci. Technol. vol. 44 (9) (2010) 3462–3467.
[34] R.A.T. Akbour, J. Douch, M. Hamdani, P. Schmitz, Transport of kaolinite colloids through quartz sand: influence of humic acid, Ca2+, and trace metals, J. Colloid Interface Sci. vol. 253 (1) (2002) 1–8.
[35] R.W. Harvey, D.W. Metge, L.B. Barber, G.R. Aiken, Effects of altered groundwater chemistry upon the pH-dependency and magnitude of bacterial attachment during transport within an organically contaminated sandy aquifer, Water Res. vol. 44 (4) (2010) 1062–1071.
[36] S. Hong, M. Elimelech, Chemical and physical aspects of natural organic matter (NOM) fouling of nanofiltration membranes, J. Membr. Sci. vol. 132 (2) (1997) 159–181.
[37] D. Grolimund, K. Barmettler, M. Borkovec, Release and transport of colloidal particles in natural porous media: 2. Experimental results and effects of ligands, Water Resour. Res. vol. 37 (3) (2001) 571–582.
[38] S.B. Roy, D.A. Dzombak, Colloid release and transport processes in natural and model porous media, Colloids Surf. A: Physicochem. Eng. Asp. vol. 107 (1996) 245–262.

[39] C. Shen, B. Li, Y. Huang, Y. Jin, Kinetics of coupled primary-and secondary-minimum deposition of colloids under unfavorable chemical conditions, Environ. Sci. Technol. vol. 41 (20) (2007) 6976–6982.
[40] S. Torkzaban, S.A. Bradford, J.L. Vanderzalm, B.M. Patterson, B. Harris, H. Prommer, Colloid release and clogging in porous media: Effects of solution ionic strength and flow velocity, J. Contam. Hydrol. vol. 181 (2015) 161–171.
[41] B. Kianfar, J. Tian, J. Rozemeijer, B. van der Zaan, T.A. Bogaard, J.W. Foppen, Transport characteristics of DNA-tagged silica colloids as a colloidal tracer in saturated sand columns; role of solution chemistry, flow velocity, and sand grain size, J. Contam. Hydrol. vol. 246 (2022), 103954.
[42] Y.S.R. Krishna, N. Seetha, S.M. Hassanizadeh, Experimental and numerical investigation of the effect of temporal variation in ionic strength on colloid retention and remobilization in saturated porous media, J. Contam. Hydrol. vol. 251 (2022), 104079.
[43] J. Zhuang, J.S. Tyner, E. Perfect, Colloid transport and remobilization in porous media during infiltration and drainage, J. Hydrol. vol. 377 (1–2) (2009) 112–119.
[44] M.W. Hahn, C.R. O'Melia, Deposition and reentrainment of Brownian particles in porous media under unfavorable chemical conditions: Some concepts and applications, Environ. Sci. Technol. vol. 38 (1) (2004) 210–220.
[45] J.J. Lenhart, J.E. Saiers, Colloid mobilization in water-saturated porous media under transient chemical conditions, Environ. Sci. Technol. vol. 37 (12) (2003) 2780–2787.
[46] T. Cheng, J.E. Saiers, Mobilization and transport of in situ colloids during drainage and imbibition of partially saturated sediments, Water Resour. Res. vol. 45 (8) (2009).
[47] S.A. Bradford, S. Torkzaban, F. Leij, J. Simunek, Equilibrium and kinetic models for colloid release under transient solution chemistry conditions, J. Contam. Hydrol. vol. 181 (2015) 141–152.
[48] Y. Wang, S.A. Bradford, J. Simunek, Release of E. coli D21g with transients in water content, Environ. Sci. Technol. vol. 48 (16) (2014) 9349–9357.
[49] M. Bendersky, J.M. Davis, DLVO interaction of colloidal particles with topographically and chemically heterogeneous surfaces, J. Colloid Interface Sci. vol. 353 (1) (2011) 87–97.
[50] R. Duffadar, S. Kalasin, J.M. Davis, M.M. Santore, The impact of nanoscale chemical features on micron-scale adhesion: crossover from heterogeneity-dominated to mean-field behavior, J. Colloid Interface Sci. vol. 337 (2) (2009) 396–407.
[51] E. Pazmino, J. Trauscht, B. Dame, W.P. Johnson, Power law size-distributed heterogeneity explains colloid retention on soda lime glass in the presence of energy barriers, Langmuir vol. 30 (19) (2014) 5412–5421.
[52] C.A. Ron, W.P. Johnson, Complementary colloid and collector nanoscale heterogeneity explains microparticle retention under unfavorable conditions, Environ. Sci.: Nano vol. 7 (12) (2020) 4010–4021.
[53] D. Paunescu, M. Puddu, J.O. Soellner, P.R. Stoessel, R.N. Grass, Reversible DNA encapsulation in silica to produce ROS-resistant and heat-resistant synthetic DNA'fossils', Nat. Protoc. vol. 8 (12) (2013) 2440–2448.
[54] R.N. Grass, J. Schälchli, D. Paunescu, J.O. Soellner, R. Kaegi, W.J. Stark, Tracking trace amounts of submicrometer silica particles in wastewaters and activated sludge using silica-encapsulated DNA barcodes, Environ. Sci. Technol. Lett. vol. 1 (12) (2014) 484–489.
[55] A. Kittilä, M. Jalali, K.F. Evans, M. Willmann, M.O. Saar, X.Z. Kong, Field comparison of DNA-labeled nanoparticle and solute tracer transport in a fractured crystalline rock, Water Resour. Res. vol. 55 (8) (2019) 6577–6595.
[56] X.-Z. Kong, et al., Tomographic reservoir imaging with DNA-labeled silica nanotracers: the first field validation, Environ. Sci. Technol. vol. 52 (23) (2018) 13681–13689.
[57] G. Mikutis, et al., Silica-encapsulated DNA-based tracers for aquifer characterization, Environ. Sci. Technol. vol. 52 (21) (2018) 12142–12152.
[58] Y. Zhang, "DNA-Encapsulated Silica Nanoparticle Tracers for Fractured Reservoir Characterization," Stanford University, 2015.
[59] Y. Zhang, T.S. Manley, K. Li, and R.N. Horne, "Uniquely identifiable DNA-embedded silica nanotracer for fractured reservoir characterization," in *Proceedings of the 41st Workshop on Geothermal Reservoir Engineering*, 2016: Stanford University Stanford, CA.
[60] C.A. Mora, et al., Ultrasensitive quantification of pesticide contamination and drift using silica particles with encapsulated DNA, Environ. Sci. Technol. Lett. vol. 3 (1) (2016) 19–23.
[61] I. Caltran, L. Rietveld, H. Shorney-Darby, S. Heijman, Separating NOM from salts in ion exchange brine with ceramic nanofiltration, Water Res. vol. 179 (2020), 115894.
[62] C. Chassagne, M. Ibanez, Hydrodynamic size and electrophoretic mobility of latex nanospheres in monovalent and divalent electrolytes, Colloids Surf. A: Physicochem. Eng. Asp. vol. 440 (2014) 208–216.
[63] Y. Tian, B. Gao, L. Wu, R. Muñoz-Carpena, Q. Huang, Effect of solution chemistry on multi-walled carbon nanotube deposition and mobilization in clean porous media, J. Hazard. Mater. vol. 231 (2012) 79–87.
[64] K.-M. Yao, M.T. Habibian, C.R. O'Melia, Water and waste water filtration. Concepts and applications, Environ. Sci. Technol. vol. 5 (11) (1971) 1105–1112.
[65] B.E. Logan, D. Jewett, R. Arnold, E. Bouwer, C. O'Melia, Clarification of clean-bed filtration models, J. Environ. Eng. vol. 121 (12) (1995) 869–873.
[66] R.W. Harvey, S.P. Garabedian, Use of colloid filtration theory in modeling movement of bacteria through a contaminated sandy aquifer, Environ. Sci. Technol. vol. 25 (1) (1991) 178–185.
[67] J.N. Ryan, M. Elimelech, Colloid mobilization and transport in groundwater, Colloids Surf. A: Physicochem. Eng. Asp. vol. 107 (1996) 1–56.
[68] N. Tufenkji, M. Elimelech, Correlation equation for predicting single-collector efficiency in physicochemical filtration in saturated porous media, Environ. Sci. Technol. vol. 38 (2) (2004) 529–536.
[69] C. Wang, et al., Retention and transport of silica nanoparticles in saturated porous media: effect of concentration and particle size, Environ. Sci. Technol. vol. 46 (13) (2012) 7151–7158.
[70] J.E. Saiers, G.M. Hornberger, L. Liang, First-and second-order kinetics approaches for modeling the transport of colloidal particles in porous media, Water Resour. Res. vol. 30 (9) (1994) 2499–2506.
[71] J.F. Schijven, S.M. Hassanizadeh, Removal of viruses by soil passage: overview of modeling, processes, and parameters, Crit. Rev. Environ. Sci. Technol. vol. 30 (1) (2000) 49–127.
[72] J. Šimůnek, M.T. van Genuchten, Modeling nonequilibrium flow and transport processes using HYDRUS, Vadose Zone J. vol. 7 (2) (2008) 782–797.
[73] C.V. Chrysikopoulos, V.E. Katzourakis, Colloid particle size-dependent dispersivity, Water Resour. Res. vol. 51 (6) (2015) 4668–4683.
[74] C.V. Chrysikopoulos, V.I. Syngouna, Effect of gravity on colloid transport through water-saturated columns packed with glass beads: modeling and experiments, Environ. Sci. Technol. vol. 48 (12) (2014) 6805–6813.
[75] S.A. Bradford, M. Bettahar, J. Simunek, M.T. Van Genuchten, Straining and attachment of colloids in physically heterogeneous porous media, Vadose Zone J. vol. 3 (2) (2004) 384–394.
[76] Z. Liu, P. Hedayati, E.J. Sudhölter, R. Haaring, A.R. Shaik, N. Kumar, Adsorption behavior of anionic surfactants to silica surfaces in the presence of calcium ion and polystyrene sulfonate, Colloids Surf. A: Physicochem. Eng. Asp. vol. 602 (2020), 125074.
[77] I.L. Molnar, W.P. Johnson, J.I. Gerhard, C.S. Willson, D.M. O'carroll, Predicting colloid transport through saturated porous media: a critical review, Water Resour. Res. vol. 51 (9) (2015) 6804–6845.
[78] J.E. Patiño, W.P. Johnson, V.L. Morales, Relating mechanistic fate with spatial positioning for colloid transport in surface heterogeneous porous media, J. Colloid Interface Sci. vol. 641 (2023) 666–674.
[79] C.A. Ron, K. VanNess, A. Rasmuson, W.P. Johnson, How nanoscale surface heterogeneity impacts transport of nano-to micro-particles on surfaces under unfavorable attachment conditions, Environ. Sci.: Nano vol. 6 (6) (2019) 1921–1931.
[80] S. Torkzaban, S.A. Bradford, Critical role of surface roughness on colloid retention and release in porous media, Water Res. vol. 88 (2016) 274–284.
[81] K. VanNess, A. Rasmuson, C.A. Ron, W.P. Johnson, A unified force and torque balance for colloid transport: predicting attachment and mobilization under favorable and unfavorable conditions, Langmuir vol. 35 (27) (2019) 9061–9070.
[82] E. Pazmino, J. Trauscht, W.P. Johnson, Release of colloids from primary minimum contact under unfavorable conditions by perturbations in ionic strength and flow rate, Environ. Sci. Technol. vol. 48 (16) (2014) 9227–9235.
[83] N. Tufenkji, M. Elimelech, Deviation from the classical colloid filtration theory in the presence of repulsive DLVO interactions, Langmuir vol. 20 (25) (2004) 10818–10828.
[84] J.E. Tobiason, Chemical effects on the deposition of non-brownian particles, Colloids Surf. vol. 39 (1) (1989) 53–75.
[85] W.P. Johnson, M. Tong, Observed and simulated fluid drag effects on colloid deposition in the presence of an energy barrier in an impinging jet system, Environ. Sci. Technol. vol. 40 (16) (2006) 5015–5021.
[86] A. Amirbahman, T.M. Olson, Transport of humic matter-coated hematite in packed beds, Environ. Sci. Technol. vol. 27 (13) (1993) 2807–2813.
[87] D. Wang, S.A. Bradford, R.W. Harvey, B. Gao, L. Cang, D. Zhou, Humic acid facilitates the transport of ARS-labeled hydroxyapatite nanoparticles in iron oxyhydroxide-coated sand, Environ. Sci. Technol. vol. 46 (5) (2012) 2738–2745.
[88] T. Cheng, J.E. Saiers, Effects of dissolved organic matter on the co-transport of mineral colloids and sorptive contaminants, J. Contam. Hydrol. vol. 177 (2015) 148–157.
[89] W.P. Johnson, B.E. Logan, Enhanced transport of bacteria in porous media by sediment-phase and aqueous-phase natural organic matter, Water Res. vol. 30 (4) (1996) 923–931.
[90] A. Amirbahman, T.M. Olson, Deposition kinetics of humic matter-coated hematite in porous media in the presence of Ca2+, Colloids Surf. A: Physicochem. Eng. Asp. vol. 99 (1) (1995) 1–10.
[91] A.A. MacKay, B. Canterbury, Oxytetracycline sorption to organic matter by metal-bridging, J. Environ. Qual. vol. 34 (6) (2005) 1964–1971.
[92] B. Pan, B. Xing, Adsorption mechanisms of organic chemicals on carbon nanotubes, Environ. Sci. Technol. vol. 42 (24) (2008) 9005–9013.
[93] M. Zhang, S.A. Bradford, J. Šimůnek, H. Vereecken, E. Klumpp, Roles of cation valance and exchange on the retention and colloid-facilitated transport of functionalized multi-walled carbon nanotubes in a natural soil, Water Res. vol. 109 (2017) 358–366.
[94] J. Nocito-Gobel, J.E. Tobiason, Effects of ionic strength on colloid deposition and release, Colloids Surf. A: Physicochem. Eng. Asp. vol. 107 (1996) 223–231.
[95] S. Torkzaban, H.N. Kim, J. Simunek, S.A. Bradford, Hysteresis of colloid retention and release in saturated porous media during transients in solution chemistry, Environ. Sci. Technol. vol. 44 (5) (2010) 1662–1669.
[96] N. Tufenkji, M. Elimelech, Breakdown of colloid filtration theory: role of the secondary energy minimum and surface charge heterogeneities, Langmuir vol. 21 (3) (2005) 841–852.
[97] W.P. Johnson, E. Pazmino, H. Ma, Direct observations of colloid retention in granular media in the presence of energy barriers, and implications for inferred mechanisms from indirect observations, Water Res. vol. 44 (4) (2010) 1158–1169.

[98] C. Shen, S.A. Bradford, T. Li, B. Li, Y. Huang, Can nanoscale surface charge heterogeneity really explain colloid detachment from primary minima upon reduction of solution ionic strength? J. Nanopart. Res. vol. 20 (2018) 1–18.

[99] B. Derjaguin, L. Landau, Theory of the stability of strongly charged lyophobic sols and of the adhesion of strongly charged particles in solutions of electrolytes, Progress in Surface Science 43 (1–4) (1993) 30–59.

[100] E. Verwey, J.T.G. Overbeek, Theory of the stability of lyophobic colloids, Journal of Colloid Science 10 (2) (1955) 224–225.